Biosensors and Bioelectronics 91 (2017) 225–231

Contents lists available at ScienceDirect

Biosensors and Bioelectronics

journal homepage: www.elsevier.com/locate/bios

Graphene-interfaced electrical biosensor for label-free and sensitive detection of foodborne pathogenic *E. coli* O157:H7

Ashish Pandey[a], Yasar Gurbuz[b], Volkan Ozguz[a], Javed H. Niazi[a,*], Anjum Qureshi[a,*]

[a] Sabanci University Nanotechnology Research and Application Center, Orta Mah., 34956 Istanbul, Turkey
[b] Faculty of Engineering and Natural Science, Sabanci University, Orhanli, Tuzla, 34956 Istanbul, Turkey

ARTICLE INFO

Keywords:
Biosensors
Graphene
Dielectric
Biochip
Foodborne pathogen
E. coli O157:H7

ABSTRACT

E. coli O157:H7 is an enterohemorrhagic bacteria responsible for serious foodborne outbreaks that causes diarrhoea, fever and vomiting in humans. Recent foodborne *E. coli* outbreaks has left a serious concern to public health. Therefore, there is an increasing demand for a simple, rapid and sensitive method for pathogen detection in contaminated foods. In this study, we developed a label-free electrical biosensor interfaced with graphene for sensitive detection of pathogenic bacteria. This biosensor was fabricated by interfacing graphene with interdigitated microelectrodes of capacitors that were biofunctionalized with *E. coli* O157:H7 specific antibodies for sensitive pathogenic bacteria detection. Here, graphene nanostructures on the sensor surface provided superior chemical properties such as high carrier mobility and biocompatibility with antibodies and bacteria. The sensors transduced the signal based on changes in dielectric properties (capacitance) through (i) polarization of captured cell-surface charges, (ii) cells' internal bioactivity, (iii) cell-wall's electronegativity or dipole moment and their relaxation and (iv) charge carrier mobility of graphene that modulated the electrical properties once the pathogenic *E. coli* O157:H7 captured on the sensor surface. Sensitive capacitance changes thus observed with graphene based capacitors were specific to *E. coli* O157:H7 strain with a sensitivity as low as 10–100 cells/ml. The proposed graphene based electrical biosensor provided advantages of speed, sensitivity, specificity and in-situ bacterial detection with no chemical mediators, represents a versatile approach for detection of a wide variety of other pathogens.

1. Introduction

Pathogenic bacteria that causes infectious diseases pose serious public health concern worldwide and contribute to significant economic losses (Paulitz and Belanger, 2001). Events such as the massive outbreak of *E. coli* O157:H7 infection occurred in Japan in 1996 (Michino et al., 1999) and recently in Europe (World Health Organization, 2011) has claimed many lives and sent shocking news around the world. Among the pathogens associated with life-threatening symptoms, the enterohemorrhagic *E. coli* bacterial strains have caused serious foodborne outbreaks (Abadias et al., 2008; Alocilja and Radke, 2003; Barreiros dos Santos et al., 2013). Detection and control of such foodborne bacterial-pathogens, such as *E. coli* serotype O157:H7 is one of the major challenges in preventing severe diseases in humans (Geng et al., 2008; Tokarskyy and Marshall, 2008; Yang and Bashir, 2008).

Recently, there has been an increasing demand for pathogen detection methods in a simple, rapid and sensitive capacity to provide rich information on pathogens, especially in resource-limited settings. A variety of complex methods, such as polymerase chain reaction (PCR)-based methods (Atrazhev et al., 2010; Soto et al., 2010), DNA microarrays (Peham et al., 2012; Rasooly and Herold, 2008), DNA sequencing technology (Li and Rothberg, 2004), ELISA (Charlermroj et al., 2013), staining (Swannell and Williamson, 1988), isolation (Hansen et al., 2009), and cell culture (Vimont et al., 2006) have been employed for pathogen detection. In all of the above methods, it is essential that the suspected samples have to be extensively processed for pathogen detection, such as cell-lysis, DNA extraction, amplification and purification (Lemarchand et al., 2005). These methods require expensive and high-precision instruments that rely on cumbersome procedures and project challenges of false positives due to cross-reactivity. Further, various fluorescent (Bruno et al., 2010; Ohk et al., 2010) or electrochemical detection (Torres-Chavolla and Alocilja, 2009) based biosensors have been developed for pathogen detection. These require secondary chemical mediators such as fluorophores or redox-agents for signal generation. Therefore, new alternative strategies are required that allow direct, in-situ and sensitive detection of bacterial-pathogens.

* Corresponding authors.
E-mail addresses: javed@sabanciuniv.edu (J.H. Niazi), anjum@sabanciuniv.edu (A. Qureshi).

http://dx.doi.org/10.1016/j.bios.2016.12.041
Received 20 October 2016; Received in revised form 1 December 2016; Accepted 15 December 2016
Available online 16 December 2016
0956-5663/

Integrating graphene nanostructures has proved to be advantageous in enhancing sensitivities of electrochemical sensors and develop new generation of biosensors. For example, the large surface area of 2D-graphene enables homogeneous functionalization of biological materials. Graphene's superior electrical properties such as, high charge-mobility at room temperature with tunable conductance makes it sensitive to a small amount of extra charges to cause a noticeable change in electronic-sensors (Yang et al., 2010). Recently, sensitive electrochemical immunosensor based on graphene-wrapped copper oxide-cysteine hybrid composite was employed for the detection of pathogenic bacteria (Pandey et al., 2017). Graphene-based other electrochemical biosensors for detection of bacterial cells have been reported that heavily rely on redox-mediators which hampers signal transduction (Hernandez et al., 2014; Tiwari et al., 2015; Wang et al., 2013). Graphene-based field effect transistors (FETs**)** have been reported to detect *E. coli* living cells (Akbari et al., 2015; Hess et al., 2011; Huang et al., 2011). Such studies emphasized on graphene-interfaced devices for detecting cells but suffer from major challenges, such as specific bio-anchoring without altering graphene electrical properties and temperature effects.

In this study, we developed a label-free graphene based electrical biosensor for sensitive and specific detection of foodborne pathogenic *E. coli* O157:H7 bacteria. This biosensor was fabricated by directly interfacing graphene-nanostructures functionalized with O157:H7-specific-antibodies that captured pathogenic bacteria on the sensor surface. We tested two distinct types of graphene nanostructures through interfacing with SiO_2-substrates, such as defect-free monolayered-graphene (MG) and less-expensive few-layered graphene nanoplatelets (GNPs). The ability of graphene's charge carrier mobility on capacitors generated sensitive electrical transduction signals is reported. The graphene-based biosensor chips designed to generate non-Faradiac electrochemical signals (capacitance/impedance) specific to pathogenic bacteria that did not require redox mediator chemicals.

2. Material and Methods

2.1. Coupling GNPs and MG on SiO_2/Si-substrates

GNPs (< 4 layers; 1–15 nm/5 nm Thickness; Surface area 700 m^2/g; 2 μm diameters, Carbon Solutions Inc., USA) were first suspended in *N, N* dimethylformamide (DMF, Sigma-Aldrich) at a concentration of 0.5 mg/ml and homogenized by ultrasonication for 5 h. The colloidal GNPs suspension was stable for 6–7 h and this suspension was subjected to spin coating followed by covalent attachment on silanized SiO_2 wafers as described in Supporting information (SI). For MG interfaced chips, chemical vapor deposition (CVD) grown defect-free monolayered-graphene coupled on SiO_2-substrates were used (Graphene platform corp., Japan) that contained defect-free monolayered-graphene (MG) on SiO_2-substrates.

2.2. Patterning of gold interdigitated microelectrodes on SiO_2-substrates interfaced with GNPs and MG and characterization

Graphene (GNPs and MG) coupled on SiO_2-substrates were subjected to patterning the gold microelectrodes to give rise to graphene-interfaced array of capacitors (electrical chip) using photolithography and the details are described in SI section. The fabricated GNPs/MG interfaced with electrical chips were characterized using scanning electron microscopy (SEM, Leo Supra 35). Raman spectra of graphene nanostructures in between the microelectrodes of capacitor arrays were obtained by Renishaw in Via Reflex Raman Microscopy with Spectrometer equipped with a 532 nm laser source.

2.3. Activation of graphene-interfaced with electrical biochip and characterization

GNPs/MG interfaced with capacitor arrays were incubated with 5 mM of 1-pyrenebutanoic acid succinimidyl ester (PASE) in methanol for 2 h and a self-assembly of PASE was formed on outermost layers of graphene-on-chips by systematic stacking that provided active functional groups for antibody immobilization. Sensors were then washed with methanol followed by water and dried. Thus obtained PASE activated sensor chips were incubated overnight with anti-*E. coli* O157:H7 antibodies (1, 3 and 5 μg/ml in PBS) at 4 °C. The chips were thoroughly washed with PBS followed by water and the extra unreacted antibodies or salts were removed. Finally, the chips were incubated with 5% bovine serum albumin (BSA) in PBS solution containing 0.1% Tween 20 to block free or unreacted functional groups on sensor surface. Immobilization of anti-*E. coli* O157:H7 on graphene-interfaced with chips were confirmed by Fourier transform infrared spectroscopy (FTIR) using Thermo scientific Nicolet™ iS™10 FT-IR Spectrometer. The contact angle measurements taken by sessile drop method that enabled determining the changes in sensor hydrophilicity favoring biological reactions on sensors.

2.4. Bacterial cultures and incubation of cells-on-chips

E. coli O157:H7 (NCTC 12900, Public Health England) with serotype O157:H7 were regenerated according to the NCTC instructions on Luria Bertani (LB) agar medium. Appropriate safety measures were taken in handling the bacteria as per the guidelines of NCTC and the details are described in SI-section. A wild-type non-specific *E. coli* strain (DH5α) was used as a negative control under identical conditions for validation. Replicate cell-suspensions ranging from 10–10^7 cells/ml were prepared freshly just before the biosensing processes. A series of *E. coli* O157:H7 cell concentrations ranging 10–10^7 cells/ml in 5 μl volumes (about one drop) were incubated on capacitor arrays functionalized with anti-*E. coli* O157:H7 antibodies for 30 min. After incubation, the sample drops on each capacitor in an array was quickly aspirated using a multichannel pipette and the chips were washed with PBS followed by a quick wash with water and dried. The *E. coli* O157:H7 cells captured by antibodies on sensor chips were examined under the optical microscope (Carl Zeiss).

2.5. Electrical measurements

Dielectric parameters (impedance/capacitance) of GNPs/MG-interfaced with chips before and after incubation with *E. coli* O157:H7 cells (10–10^7 cells/ml) was measured against the applied frequency from 40 Hz and 7 MHz using a Karl Süss PM-5 RF Probe Station and Agilent 4294 A impedance analyzer calibrated using SOLT (short-open-load-through) process. Specificity tests were conducted with GNPs/MG interfaced chip sensors against *E. coli* O157:H7 serotype and a non-pathogenic *E. coli* (DH5α) in at least two concentrations (10^2 and 10^4 cells/ml) and measured changes in capacitance values from replicate sensors (n=3) as a function of varying AC frequency. All measurements were performed in at least triplicates, the average values were plotted and the standard deviations are shown as errors. Percent relative standard deviation (%RSD) was calculated to be < 11% from the experimental data.

The time needed for dipoles on a cell in an electric field to relax was determined by the relaxation time, which is defined by its characteristics frequency (f_c) using below Eq. (1),

$$f_c = 1/2\pi\tau \quad (1)$$

where, τ is the relaxation time (Pethig and Kell, 1987). Analysis of dispersion characteristic frequency and relaxation time dependent upon the cells' concentration was calculated using Eq. (1).

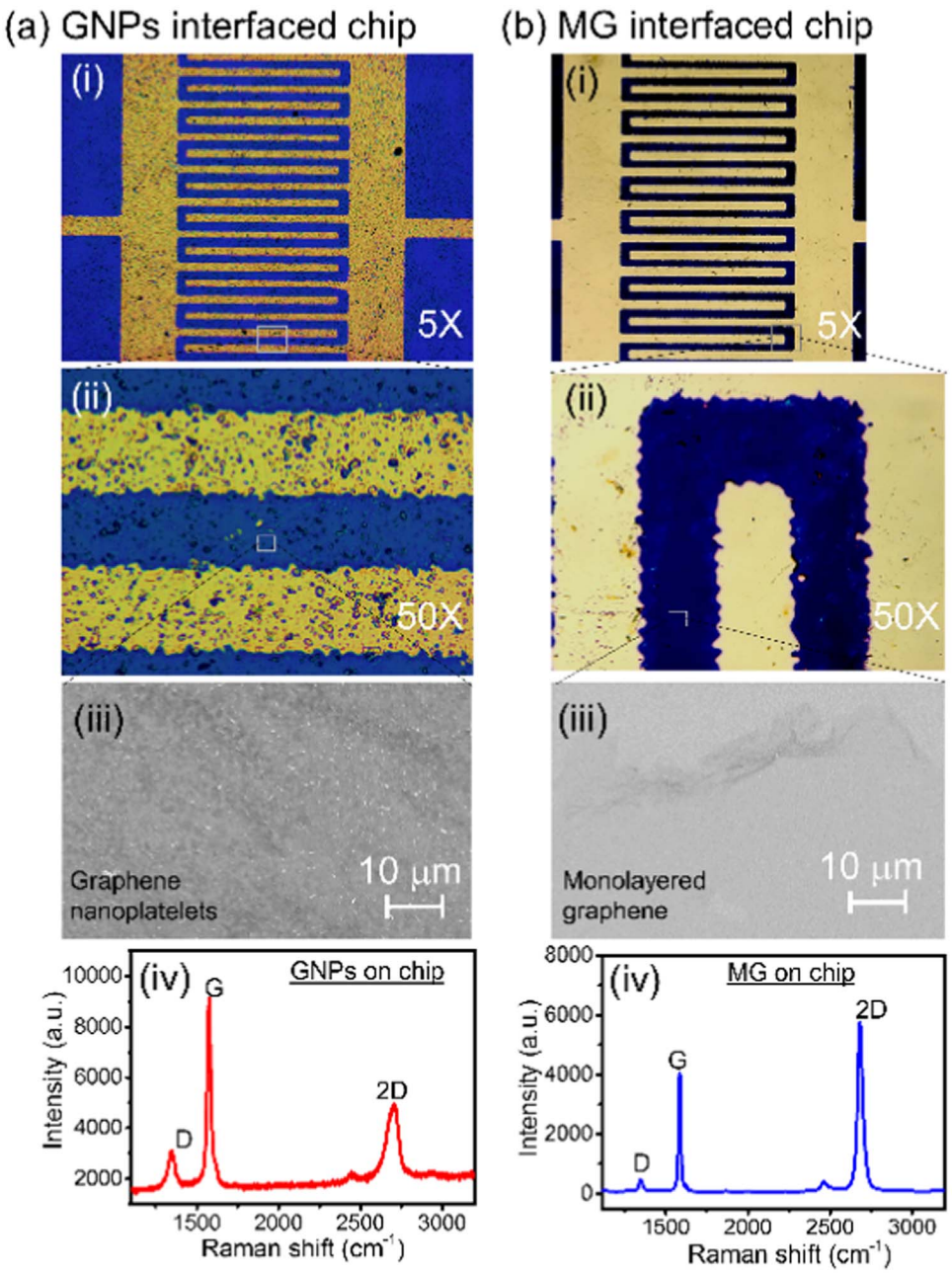

Fig. 1. Characterization of sensor chips. (a) Optical micrographs of GNPs-interfaced chip at different magnifications, such as (i) 5X and (ii) 50 X. (iii) A portion of the sensor in between the gold microelectrodes was characterized by SEM images showing distribution of spin-coated GNPs. (iv) The same substrate was also analyzed by Raman spectra that indicated presence of a few layers of GNPs. (b) MG-interfaced chip at different magnifications, such as (i) 5X and (ii) 50X (i-ii). (iii) A portion of the sensor in between the gold microelectrodes was characterized by SEM showing monolayered graphene, which was also characterized by (iv) Raman spectra.

3. Results and discussion

3.1. Characterization of GNPs and MG interfaced with electrical biosensor chips

Graphene-interfaced with electrical biosensor chips comprised of graphene networks in between the gold interdigitated microelectrodes were fabricated by standard photolithography on two substrates, such as; (i) GNPs coupled by spin-coating (GNPs interfaced chip) and (ii) CVD grown monolayered-graphene (MG interfaced chip) on SiO_2-substrates. These two substrates were utilized for determining their sensitivity to detecting pathogenic bacteria. Optical micrographs of fabricated GNPs and MG-interfaced chips are shown in Fig. 1a–b(i–ii). SEM images of GNPs and MG in between the microelectrodes of chips confirmed the presence of a few layers of GNPs and MG distributed on sensor chip surface, respectively (Fig. 1a(iii) and 1b(iii)). GNPs appeared uniformly distributed but provided rough surfaces on and in between the microelectrodes of chips due to their multi-layers compared to MG on SiO_2-substrate (Fig. 1a–b(i–ii)). Raman spectra of GNPs on chip showed 2D < G, which is attributed to the presence of a few layers of graphene on sensor surface (Fig. 1a(iv)). Raman spectra of MG on sensor surface showed that 2D > G, indicating the presence of defect-free MG layer on chip which was also clearly evident from the SEM image (Fig. 1b(iii–iv)).

GNPs/MG-chips were functionalized with anti-*E. coli* O157:H7 antibodies through PASE linker and confirmed by FTIR spectra and contact angle measurements and the related details are described in Supporting information (SI) section (Fig. 2a, Fig. S1, S2 and Table S1). Attachment of PASE on graphene likely to have occurred because pyrene tetra-rings in PASE resembled a honeycomb-like structure,

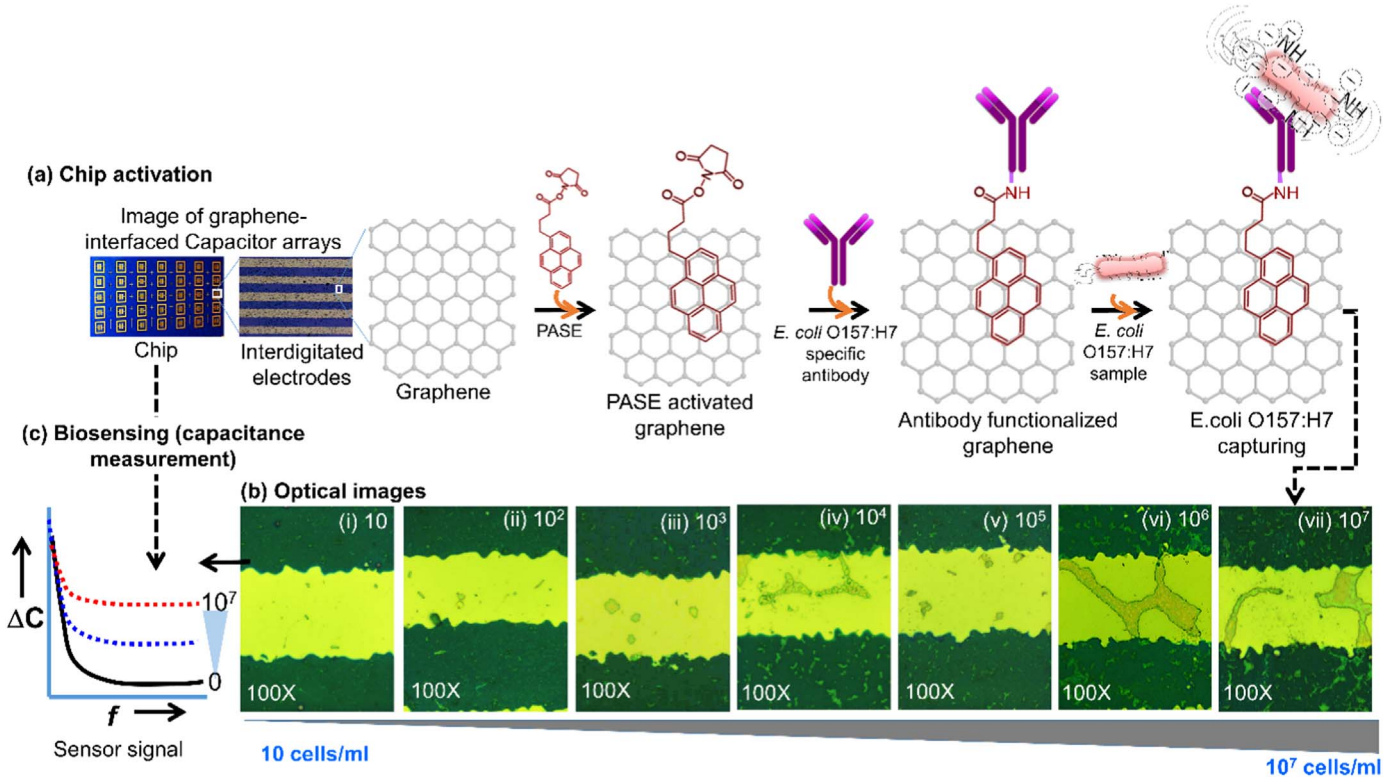

Fig. 2. (a) Photographic images of a real graphene-interfaced chip and the process of PASE activation and antibody immobilization. (b) Optical microscopic images of captured target *E. coli* O157:H7 cells on graphene-interfaced chips through specific antibodies covalently attached on chip surfaces. (c) Biosensing of *E. coli* O157:H7 through measuring capacitance change between gold microelectrodes of chips.

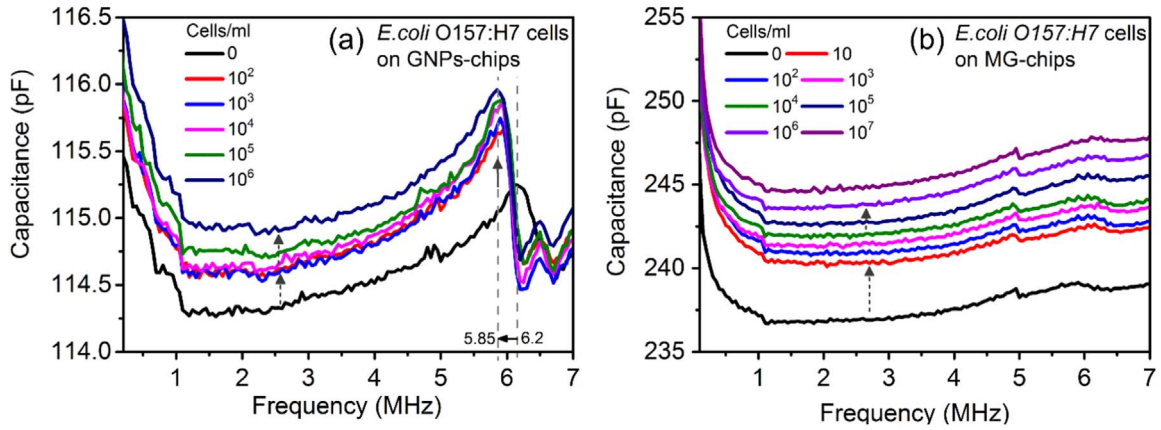

Fig. 3. Capacitance profiles of (a) GNPs- and (b) MGinterfaced-capacitor sensors with different concentrations of *E. coli* O157:H7 cells as a function of applied AC frequency. The dashed-arrows indicate cell-density dependent increase in the sensor signals.

which promoted stacking on outermost surfaces of GNPs and MG by π-π interaction. While the other terminal in PASE molecules extended free NHS-ester group, enabling covalent attachment with amino groups of antibodies specific to *E. coli* O157:H7 pathogenic bacteria (Fig. 2a).

Electrical signals from chips significantly enhanced when they were interfaced with either GNPs or MG compared with the control (no graphene) (Fig. S3). MG interfaced chips showed enhanced capacitance response which was attributed due to the presence of a monolayered-graphene with fewer defects in its structure compared with blank or GNPs interfaced chips (Fig. 1a(iii), b(iii) and Fig. S3). The increased capacitance response evidently showed that graphene-layers successfully formed conductive networks between the gold electrodes, as compared to chip responses with no graphene. Capacitor surface (control, without graphene/antibodies) initially was weakly charged, which then transformed into a significantly enhanced charged surface while in presence of graphene (GNPs/MG). Here, the presence of mono-layered and defect-free form of MG on capacitors promoted the sensitivity to immobilized antibodies at different concentrations (Fig. S4a–b). Cumulative charges resulting from 5 μg/ml of antibodies on an area of 3 mm^2 appeared to be maximum capacity of each fabricated GNPs and MG-interfaced capacitor chips and the detailed results are described in SI section.

The antibody-functionalized GNPs and MG-interfaced capacitor arrays were incubated with a series of *E. coli* O157:H7 cell concentrations (0–10^7 cells/ml) (Fig. 2a–b). Capturing of cells on sensor surface by *E. coli* O157:H7-specific antibodies was confirmed by examining under the optical microscope that showed clear cell-density dependent attachment (Fig. 2b). Optical images also revealed that the antibodies were also found immobilized on gold surfaces, indicating that PASE activation also occurred non-specifically on gold surfaces probably by

physical adsorption that persisted to washings.

3.2. Detection of E. coli O157:H7 on electrical chips interfaced with GNPs and MG

The capacitance change as a function of different concentrations of *E. coli* O157:H7 cells on GNPs and MG-interfaced sensor are shown in Fig. 3a–b. Changes in capacitance profiles from sensor chips captured with O157:H7 cells (0–10^7 cells/ml) were measured against the applied AC frequency (40 Hz-7 MHz) (Fig. 3a–b). An appropriate applied frequency of 6 MHz was selected based on the prominent dispersion peak found in GNPs-chip and extrapolated the effective capacitance changes with respect to responses of GNPs/MG chips to varying antibodies concentrations (Fig. S5).

Capacitance responses from GNPs and MG-interfaced sensors tended to increase with increased concentrations of cells captured by specific antibodies present on the sensor surfaces. Changes in sensor responses specific to *E. coli* O157:H7 are postulated to occur due to the following reasons. First, the antibodies functionalized on sensors were specific to pathogenic *E. coli* O157:H7 bacteria. Second, the net negative charges from the outer cell-wall/membrane components, such as proteins and phospholipids form the ionisable acidic and basic groups contribute to the overall net negative charges on bacterial-surface. Finally, third, the above cellular features induce changes in the carrier hole density in graphene upon their capturing of cells-on-chips.

Results of GNPs-interfaced chip showed a unique signature in dispersion curves as a function of applied AC frequency after capturing *E. coli* O157:H7 cells (Fig. 3a). At low frequencies (0–2.5 MHz), cells seemed to develop resistance probably due to cell membrane insulation from an external field, thus decreasing capacitance signal at lower frequency range can be seen. However, dynamic increase in capacitance dispersion curves occurred at higher frequencies (4–7 MHz) as the cell numbers increased when compared to control chip response in absence of antibodies (Fig. 3a and Fig. S4). The dispersion peak at 6.2 MHz with control chip (with only antibodies) tended to shift toward lower frequency of 5.85 MHz upon capturing with 10^2–10^6 *E. coli* O157:H7 cells/ml (Fig. 3a). This result suggested that capacitance dispersion response of sensors was dependent on the permittivity of induced cell-surface charges with the applied frequency of an electric field. Shift in dispersion peaks is a characteristic feature of GNPs-interfaced chips captured with *E. coli* O157:H7 cells under defined optimized conditions. At higher frequencies, the charges on cells-on-chip allow electric field to penetrate into the cell until reaching to a sufficiently tolerable frequency, during which the cells-on-chip dielectrically polarized as a spheroid composed of molecular dipoles resulting in a short-circuiting effect (Pethig and Kell, 1987). The dipole polarization of cells may fall and rise with increasing frequency leading to a dispersion curve as evidenced in Fig. 3a. The shift in dispersion peak from characteristic frequency of 6.2 MHz with antibody to 5.85 MHz upon captured *E coli* O157:H7 cells also indicated its origination from permanent and induced dipoles on cells surfaces aligning to an electric field.

The time needed for electrical field induced dipoles on a cell-surface to relax (relaxation time) can be defined by its characteristics frequency from Eq. (1) (Pethig and Kell, 1987). Therefore, it is expected that the relaxation time of cells-on-GNPs chip should increase as the cell-density increases on sensors. Table S2 shows the relaxation time of cells with respect to its characteristic frequency calculated based on dispersion profile from O157 cells-on-GNPs interfaced chips. It is clear from the results that the relaxation time of *E. coli* O157 cells-on-GNPs increased with increasing cell-density from 10^2 to 10^6 cells/ml, indicating effective mobility of the surface charges/ions (dipole moments) with applied electric field (Table S2). Increase in cell-density on chips provided larger volume on sensor surface that probably lead to changes in intermolecular/cellular motion due to anisotropic change with applied AC frequency (f_c).

The MG-interfaced chip showed *E. coli* O157:H7 cell-density dependent increase in capacitance responses from as low as 10 to 10^7 cells/ml as compared with GNPs-interfaced chip responses (Fig. 3a–b). The sensitivity of MG-chip was associated with the presence of defect-free monolayered-graphene nanostructures. Such materials show no electrostatic screening effect as compared with multilayer-graphene with strongest electrostatic correlation when the electrode is charged (Ji et al., 2014). Therefore, MG-interfaced chip showed high sensitivity with no capacitance dispersion peak or peak shift unlike GNPs-chip, proving MG-interfaced chips served as an excellent sensor platform for detecting *E. coli* O157:H7 cells.

Capacitive responses of the presented sensors are resulted from the antibody-bacterial interactions on graphene surface. Such interactions may induce sensitive changes in conductivity if defect-free MG networks present in between the gold electrodes than the multi-layered GNPs. Therefore, efficient charge redistribution and recombination within these conductive networks of MG-interfaced chips provided greater sensitivity to varying cell numbers (Fig. 3a–b). Capacitance changes over low frequency are related to double-layer effects on sensor surface (Taylor and Macdonald, 1987), while changes at high frequencies could be derived from the adsorption of cells on electrode surface (Fig. 3a–b). Therefore, capacitance responses over low or high frequency can be attributed to the formation of a double-layer or adsorption of captured target cells, respectively by the graphene networks in between the gold electrode surfaces.

The experimental data can be well represented by a simple equivalent electrical circuit of a cell as shown in Fig. 4a. Here, C_m is the membrane capacitance with its corresponding resistance R_m.The equivalent circuit of the GNPs/MG interfaced chips used in this study is shown in Fig. 4b. In this circuit diagram, R_{f1} and R_{f2} are the ohmic resistances in between the electrodes, L_1 and L_2 are the magnetic coupling between the electrodes (self-inductances) and C, the capacitance between the microelectrodes through GNPs/MG and gold surfaces, including the fringing capacitance of the microelectrodes into the air. The capacitance C_m is associated with the cell-wall/surface on the electrodes corresponding to the resistance R_3. The antibody probe immobilization on graphene and cells binding on graphene sensor surface influence changes in the charge density (dielectric changes) on microelectrodes through polarization of cell-surface charges, intracellular bioactivity and dipoles induced by cellular electronegativity that contributed to overall changes in surface conductivity and capacitive responses of sensors.

Sensor response data were extrapolated at a specific frequency to establish a linear relationship between capacitance change (ΔC) and varying number of *E. coli* O157:H7 cells that showed sensitivity and dynamic range of GNPs (10^2–10^6 cells/ml) and MG-interfaced chips (10–10^7 cells/ml) (Fig. 5a). It is clear that MG interfaced chips provided more sensitivity in detecting pathogenic bacteria compared to GNP interfaced chips (Fig. 5a). GNPs interfaced chips appeared rough with limited surface area for antibodies to capture cells, because the antibodies were localized on the peripheral region of intermittent outermost GNPs layers on sensors. The sensitivity of MG-chips was

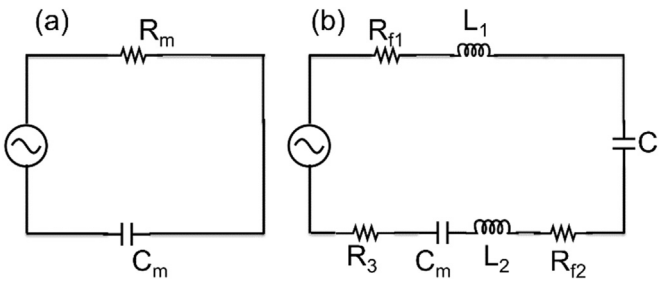

Fig. 4. Equivalent circuit of (a) a bacterial cell with R_m and C_m are the membrane resistance and capacitance, respectively and (b) graphene-interfaced biochip with R_{f1}, R_{f2} and C represent ohmic resistances and capacitance in between the electrode fingers.

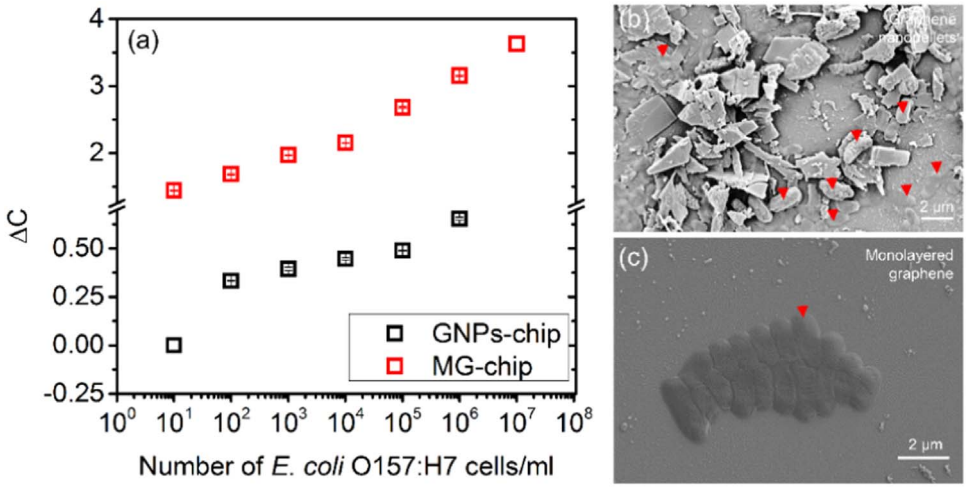

Fig. 5. (a) Relative changes in average capacitance (ΔC) values from replicate sensors (n=3, percent standard deviation, %RSD of < 2.2%) as a function of varying number of *E. coli* O157:H7 cells/ml at frequency ~5.85–6 MHz on GNPs (ΔC < 1, black) and MG (ΔC > 1, red) interfaced chips, respectively. (b and c) SEM images of *E. coli* O157:H7 cells captured by antibodies functionalized on GNPs and MG-interfaced sensor surfaces, respectively. (For interpretation of the references to color in this figure legend, the reader is referred to the web version of this article.)

therefore associated with the uniform large surface area of monolayered-defect free MG providing smooth topography and easy access for surface-antibodies to bind cells (Fig. 5b–c).

3.3. Sensor specificity

The GNPs and MG interfaced chips were designed to specifically capture O157:H7 strain of *E. coli*. Considering that other wild-type *E. coli* strains share more than 90% similarity with O157:H7 strain and therefore, it was imperative to test the sensor chips with a wild-type non-pathogenic *E. coli* strain. In this study, *E. coli* DH5α strain was used as a negative control strain on GNPs and MG interfaced chips (10^2 and 10^4 cells/ml) under identical conditions as described for *E. coli* O157:H7 cells. Specificity test results revealed no significant increase in capacitance responses with a non-pathogenic *E. coli* DH5α strain, indicating high specificity of the developed sensors for *E. coli* O157:H7 serotype (Fig. 6a–b). This specificity originated from the embedded antibodies that were highly specific to O157:H7 strain. Interestingly, the characteristic dispersion peaks in GNPs interfaced chip response profile did not shift with non-specific *E. coli* DH5α cells as it was seen with O157:H7 strain, but remained superimposed with blank response peak (with no cells). However, a small loss of capacitance with GNPs-chips occurred with non-specific cells that could be associated with heterogeneous and non-uniform distribution of GNPs on chips.

Pathogenic *E. coli* strains including strain O157:H7 are evolved from a common wild-type ancestor and therefore share a majority of characteristics of wild-type *E. coli* (Wick et al., 2005). Specific detection of pathogenic O157:H7 from the wild-type is a challenging task. However, detection of a common *E. coli* strains has been well established. For example, FET sensors in which CVD-grown graphene in between the electrodes was previously utilized to sensitively detect at the level of 10 cells/ml concentrations (Huang et al., 2011). Quartz crystal microbalance (QCM) sensor has been utilized in conjunction with beacon magnetic nanoparticles and colloidal gold to sensitively detect *E. coli* cells with a detection limit of 23 CFU/ml (Shen et al., 2011). Several reports on Fardiac approach based electrochemical impedimetric sensors were reported for specifically detecting *E. coli* O157:H7 serotype (dos Santos et al., 2013; Li et al., 2011). Li et al. presented electrochemical biosensor which is able to discriminate between 10^2 and 10^5 *E. coli* O157:H7 cells/ml (Li et al., 2011). Such studies reported the sensitive detection of pathogenic O157:H7 strain but the intra-species specificity remains to be still unclear. Recently, electrochemical sensor based on gold nanoparticles modified graphene paper provided detection of *E. coli* O157:H7 with a wide linear range (1.5×10^2–1.5×10^7 cells/ml). Similarly, an another study involving graphene nanohybrids in electrochemical sensor demonstrated specific and sensitive detection of *E. coli* O157:H7 at a range of 10–10^8 cells/ml (Tiwari et al., 2015; Wang et al., 2013). Such biosensors are

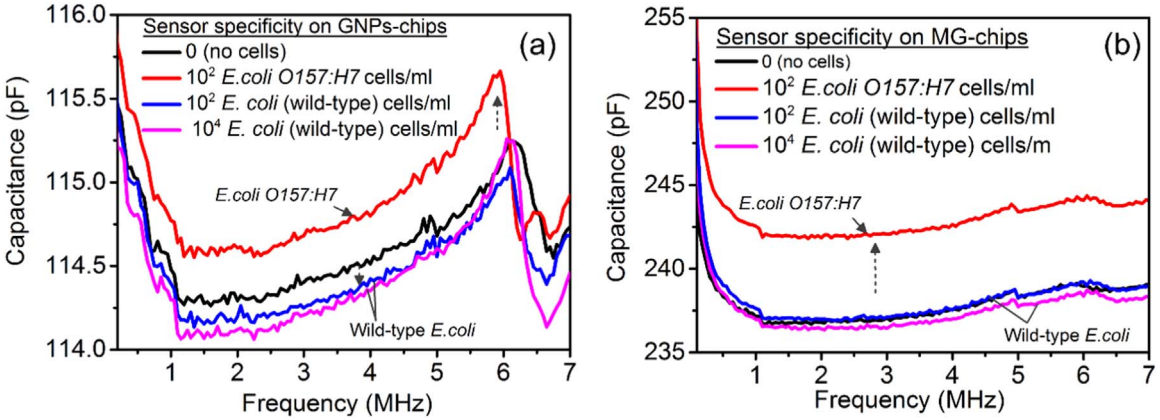

Fig. 6. Specificity tests with graphene-interfaced chip sensors conducted against pathogenic *E. coli* O157:H7 serotype and non-pathogenic *E. coli* (DH5α) using (a) GNPs and (b) MG interfaced chip sensors. Each bacterial strain was tested with at least two concentrations (10^2 and 10^4 cells/ml) and measured changes in capacitance values from replicate experiments (n=3) as a function of varied AC frequency shown in x–axis.

although highly specific to *E. coli* O157:H7 serotype, but they heavily rely on participation of a secondary redox mediating chemical in order to generate the signal. Therefore, in this study, the developed biosensor was designed to specifically detect *E. coli* O157:H7 serotype without the requirement of interfering redox chemicals to generate the signal, through simply measuring the specific changes in capacitance under applied AC electrical field. Further, the sensitivity was enhanced by interfacing sensors with monolayered-graphene in between the gold microelectrodes of capacitors that yielded a detection limit of 10–10^7 cells/ml. Sensitive signals can be measured using the developed sensor upon incubation (30 min) of a tiny droplet (5 μl) of sample containing *E. coli* O157:H7 cells on antibody functionalized capacitor arrays. The shelf-life of antibody functionalized chips stored at 4 °C can last for at least 4 weeks. The developed biosensor exploits the unique electrical properties of graphene that provided advantages of sensitivity, speed, specificity and in-situ bacterial detection with no chemical mediators unlike in most of the reported biosensors for bacteria detection in the literature. However, the quality of graphene and its distribution and adherence on sensors and batch to batch variations is still challenging for better sensor performance.

4. Conclusion

Most *E. coli* strains are harmless, but some strains of *E. coli* produce toxins causing sickness that usually trigger haemorrhagic diarrhoea, fever and vomiting. Therefore, there is an increasing demand for a simple, rapid and sensitive method for pathogen detection in suspected food samples. Introducing graphene through interfacing with electrical chip sensors could overcome challenges related to the existing detection methods. We here reported on development of a label-free graphene-interfaced capacitor chip that mainly functions on the principles of dielectric changes (capacitance/impedance) after capturing pathogenic bacterial cells on sensor chips interfaced with graphene nanostructures. The fabricated graphene based label-free electrical chip platform was designed to sensitively detect pathogenic *E. coli* O157:H7 bacteria without chemical mediators. Interfacing capacitor sensors with defect-free MG and GNPs facilitated sensitive detection of bacteria to as low as 10–100 cells/ml. The sensitivity of developed MG and GNPs biosensors was ~4 pF and ~1 pF in terms of change in biosensor signal per unit change in analyte concentration of 10–100 cells/ml, respectively. However, a trade-off between the two distinct nature of graphene nanostructures interfaced with electrical biosensors, where defect-free MG provided greater sensitivity (10 cells/ml) but difficult to maintain defect-free nanostructure on sensors and expensive, as compared with those sensors interfaced with GNPs (minimum sensitivity=100 cells/ml). However, both capacitive sensing platforms developed in this study can serve as powerful tools for preventing epidemic associated with contagious pathogenic bacteria like *E. coli* O157:H7.

Acknowledgements

This work was support by the Scientific and Technological Research Council of Turkey (TUBITAK) to author AQ with Project Grant No. 114E101.

Appendix A. Supporting information

Supplementary data associated with this article can be found in the online version at doi:10.1016/j.bios.2016.12.041.

References

Abadias, M., Usall, J., Anguera, M., Solsona, C., Viñas, I., 2008. Int. J. Food Microbiol. 123 (1–2), 121–129.
Akbari, E., Buntat, Z., Kiani, M.J., Enzevaee, A., Khaledian, M., 2015. Int. J. Environ. Anal. Chem. 95 (9), 847–854.
Alocilja, E.C., Radke, S.M., 2003. Biosens. Bioelectron. 18 (5–6), 841–846.
Atrazhev, A., Manage, D.P., Stickel, A.J., Crabtree, H.J., Pilarski, L.M., Acker, J.P., 2010. Anal. Chem. 82 (19), 8079–8087.
Barreiros dos Santos, M., Agusil, J.P., Prieto-Simón, B., Sporer, C., Teixeira, V., Samitier, J., 2013. Biosens. Bioelectron. 45 (0), 174–180.
Bruno, J., Carrillo, M., Phillips, T., Andrews, C., 2010. J. Fluor. 20 (6), 1211–1223.
Charlermroj, R., Himananto, O., Seepiban, C., Kumpoosiri, M., Warin, N., Oplatowska, M., Gajanandana, O., Grant, I.R., Karoonuthaisiri, N., Elliott, C.T., 2013. Plos One 8 (4).
Geng, P., Zhang, X., Meng, W., Wang, Q., Zhang, W., Jin, L., Feng, Z., Wu, Z., 2008. Electrochim. Acta 53 (14), 4663–4668.
Hansen, W.L.J., Bruggeman, C.A., Wolffs, P.F.G., 2009. J. Clin. Microbiol. 47 (8), 2629–2631.
Hernandez, R., Valles, C., Benito, A.M., Maser, W.K., Rius, F.X., Riu, J., 2014. Biosens. Bioelectron. 54, 553–557.
Hess, L.H., Jansen, M., Maybeck, V., Hauf, M.V., Seifert, M., Stutzmann, M., Sharp, I.D., Offenhäusser, A., Garrido, J.A., 2011. Adv. Mater. 23 (43), 5045–5049.
Huang, Y.X., Dong, X.C., Liu, Y.X., Li, L.J., Chen, P., 2011. J. Mater. Chem. 21 (33), 12358–12362.
Ji, H.X., Zhao, X., Qiao, Z.H., Jung, J., Zhu, Y.W., Lu, Y.L., Zhang, L.L., MacDonald, A.H., Ruoff, R.S., 2014. Nat. Commun. 5.
Lemarchand, K., Berthiaume, F., Maynard, C., Harel, J., Payment, P., Bayardelle, P., Masson, L., Brousseau, R., 2005. J. Microbiol. Methods 63 (2), 115–126.
Li, D.J., Feng, Y.Y., Zhou, L., Ye, Z.Z., Wang, J.P., Ying, Y.B., Ruan, C.M., Wang, R.H., Li, Y.B., 2011. Anal. Chim. Acta 687 (1), 89–96.
Li, H., Rothberg, L.J., 2004. Anal. Chem. 76 (18), 5414–5417.
Michino, H., Araki, K., Minami, S., Takaya, S., Sakai, N., Miyazaki, M., Ono, A., Yanagawa, H., 1999. Am. J. Epidemiol. 150 (8), 787–796.
Ohk, S.H., Koo, O.K., Sen, T., Yamamoto, C.M., Bhunia, A.K., 2010. J. Appl. Microbiol. 109 (3), 808–817.
Pandey, C.M., Tiwari, I., Singh, V.N., Sood, K.N., Sumana, G., Malhotra, B.D., 2017. Sens. Actuators B: Chem. 238, 1060–1069.
Paulitz, T.C., Belanger, R.R., 2001. Annu. Rev. Phytopathol. 39, 103–133.
Peham, J.R., Recnik, L.M., Grienauer, W., Vellekoop, M.J., Nohammer, C., Wiesinger-Mayr, H., 2012. Micro. Technol. 18 (3), 311–318.
Pethig, R., Kell, D.B., 1987. Phys. Med. Biol. 32 (8), 933–970.
Rasooly, A., Herold, K.E., 2008. Foodborne Pathog. Dis. 5 (4), 531–550.
dos Santos, M.B., Agusil, J.P., Prieto-Simon, B., Sporer, C., Teixeira, V., Samitier, J., 2013. Biosens. Bioelectron. 45, 174–180.
Shen, Z.Q., Wang, J.F., Qiu, Z.G., Jin, M., Wang, X.W., Chen, Z.L., Li, J.W., Cao, F.H., 2011. Biosens. Bioelectron. 26 (7), 3376–3381.
Soto, E., Bowles, K., Fernandez, D., Hawke, J.P., 2010. Dis. Aquat. Org. 89 (3), 199–207.
Swannell, R.P.J., Williamson, F.A., 1988. FEMS Microbiol. Lett. 53 (6), 315–324.
Taylor, D.M., Macdonald, A.G., 1987. J. Phys. D Appl. Phys. 20 (10), 1277–1283.
Tiwari, I., Singh, M., Pandey, C.M., Sumana, G., 2015. Sens. Actuators B: Chem. 206, 276–283.
Tokarskyy, O., Marshall, D.L., 2008. Food Microbiol. 25 (1), 1–12.
Torres-Chavolla, E., Alocilja, E.C., 2009. Biosens. Bioelectron. 24 (11), 3175–3182.
Vimont, A., Vernozy-Rozand, C., Montet, M.P., Lazizzera, C., Bavai, C., Delignette-Muller, M.L., 2006. Appl. Environ. Micro. 72 (1), 261–268.
Wang, Y.X., Ping, J.F., Ye, Z.Z., Wu, J., Ying, Y.B., 2013. Biosens. Bioelectron. 49, 492–498.
Wick, L.M., Qi, W.H., Lacher, D.W., Whittam, T.S., 2005. J. Bacteriol. 187 (5), 1783–1791.
World Health Organization, 2011. World Health Organization, 2011, ⟨http://www.who.int/csr/don/2011_2006_2002/en/index.html⟩.
Yang, L., Bashir, R., 2008. Biotechnol. Adv. 26 (2), 135–150.
Yang, W., Ratinac, K.R., Ringer, S.P., Thordarson, P., Gooding, J.J., Braet, F., 2010. Angew. Chem. Int. Ed. 49 (12), 2114–2138.